



Figures and figure supplements

Midkine is a dual regulator of wound epidermis development and inflammation during the initiation of limb regeneration

Stephanie L Tsai et al

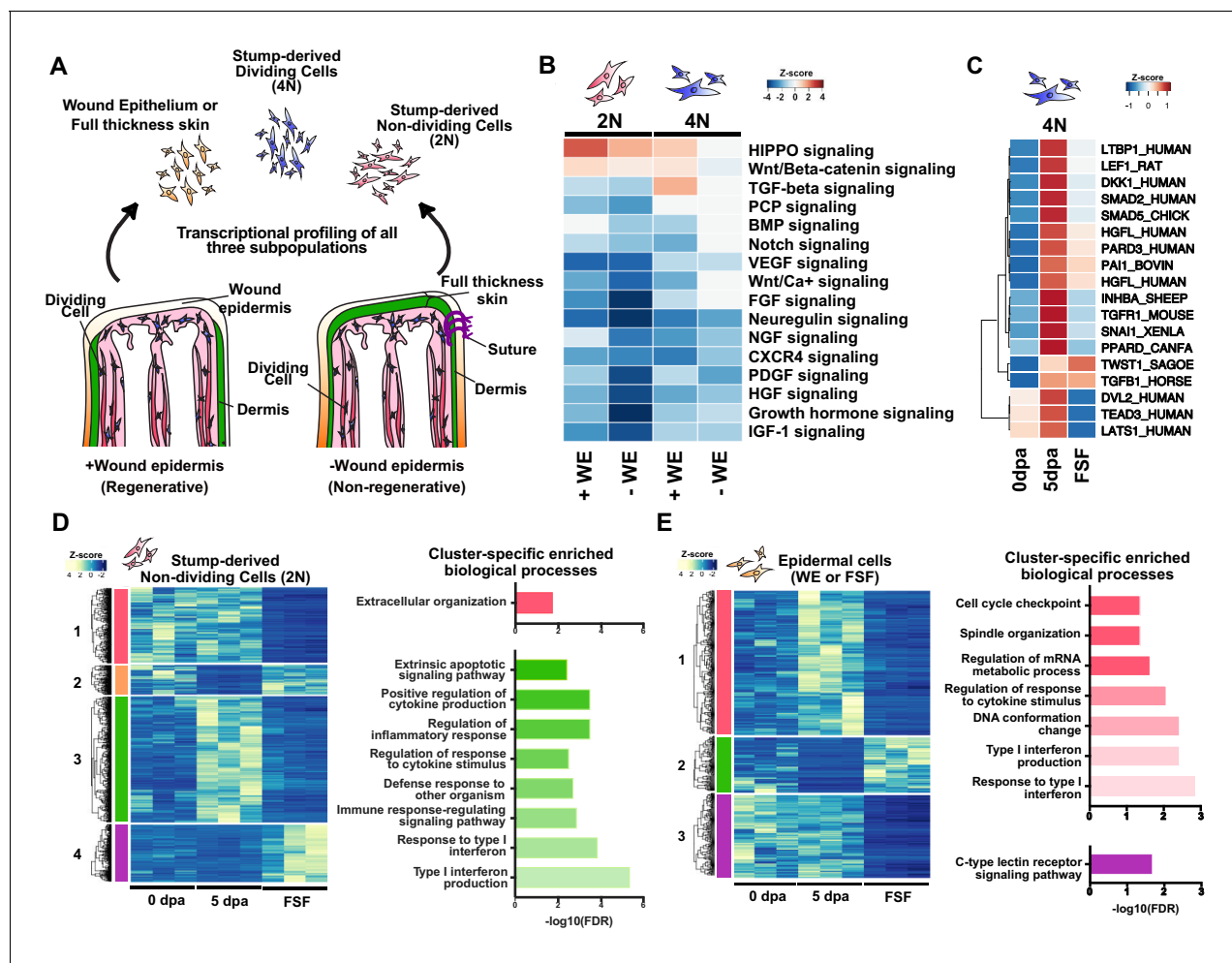


Figure 1. The early wound epidermis modulates inflammation, ECM remodeling, and tissue histolysis. (A) Design of transcriptional profiling experiment. (B) Heatmap of Ingenuity Pathway Analysis (IPA) Z-score predictions for changes in signaling pathways in injured non-epithelial stump tissues (2N and 4N) in regenerative and full skin flap conditions. (C) Heatmap of normalized transcript levels of components/regulators of the canonical Wnt, TGF-beta, and HIPPO signaling pathways in dividing cells (4N). (D–E) Heatmaps and cluster-specific enriched biological processes of differentially expressed annotated transcripts in stump-derived non-dividing cells (2N) (D) and epidermal cells of the full skin flap (E) in regenerating vs. full skin flap conditions reveals global dysregulation of inflammation, ECM regulation, and tissue histolysis. Differentially expressed transcripts can be found in **Supplementary files 1–3**. Representative histological images of full skin flap sutured vs. normal regenerating limbs, PCA analysis of the samples, as well as enriched biological processes and related differentially expressed transcripts are shown in **Figure 1—figure supplement 1**. Z-score predictions shown in B from the IPA analysis are available in **Figure 1—source data 1**.

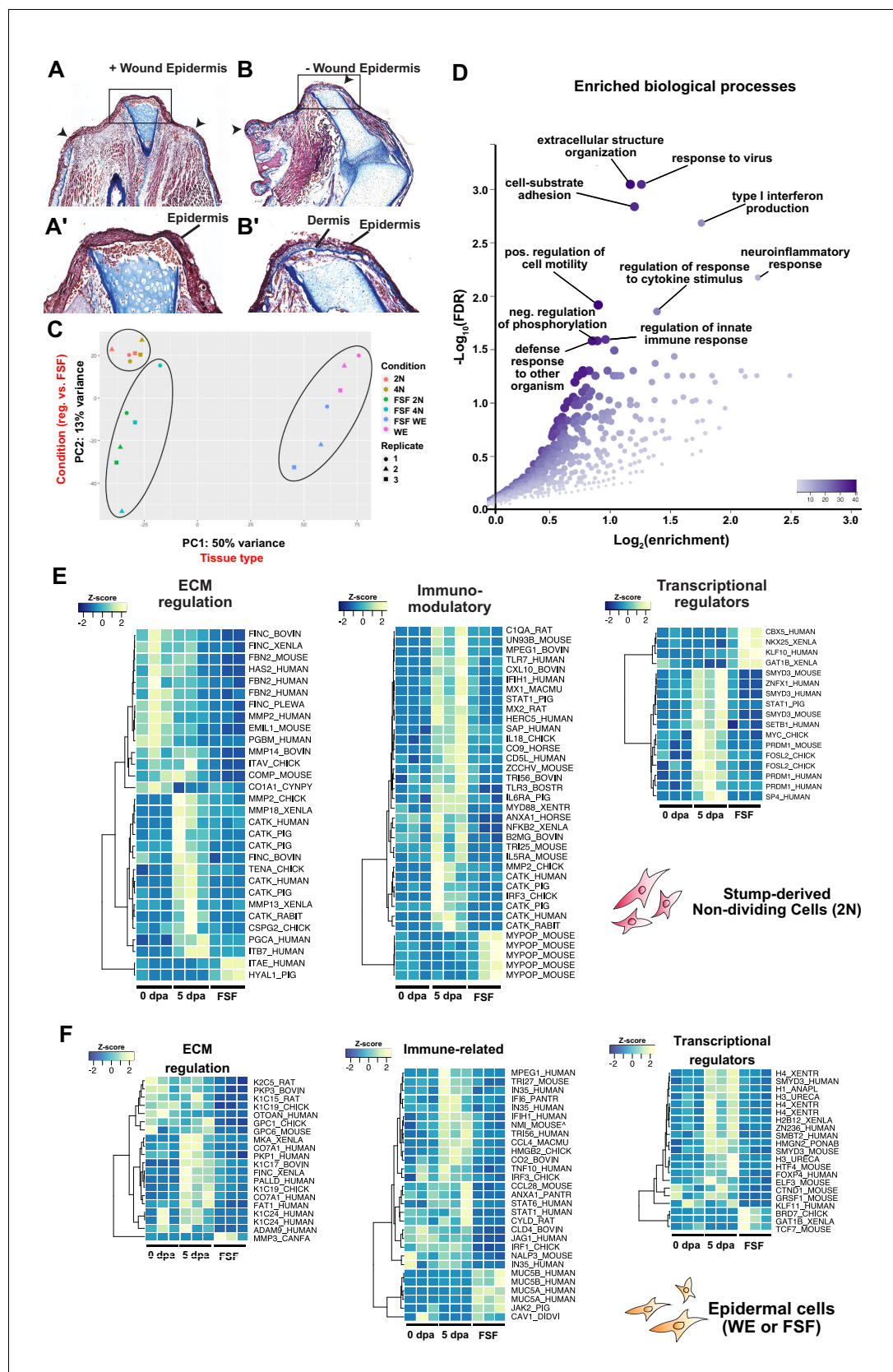


Figure 1—figure supplement 1. Sequencing of full skin flap sutured limbs reveals global dysregulation of ECM regulation, inflammation, and tissue histolysis. (A–B') Representative picro-mallory stained sections of normal regenerating and full skin flap sutured limbs. Full skin flap sutured limbs

Figure 1—figure supplement 1 continued on next page

Figure 1—figure supplement 1 continued

contain the extra dermal layer of skin tissue. Arrowheads demarcate the amputation plane. (C) Principal component analysis (PCA) of sequenced samples (5 dpa 2N, 5 dpa 4N, 5 dpa WE, FSF 2N, FSF 4N, FSF WE) based on the top 500 most highly expressed genes reveals separation along PC1 by tissue type and PC2 by condition. (D) Plot of enriched GO biological processes from all differentially expressed transcripts in non-dividing cells in full skin flap sutured limbs. (E) Heatmaps of normalized transcripts per million (TPM) values of annotated differentially expressed transcripts involved in ECM regulation, inflammation, or transcriptional regulation in non-dividing cells within regenerating stump tissues. (F) Heatmap of normalized TPM levels of annotated differentially expressed transcripts that are ECM regulators, immunomodulators, and transcriptional regulators in epithelial cells of full skin flap sutured limbs. dpa, days post-amputation, WE, wound epidermis, FSF, full skin flap, FDR, false discovery rate; ECM, extracellular matrix.

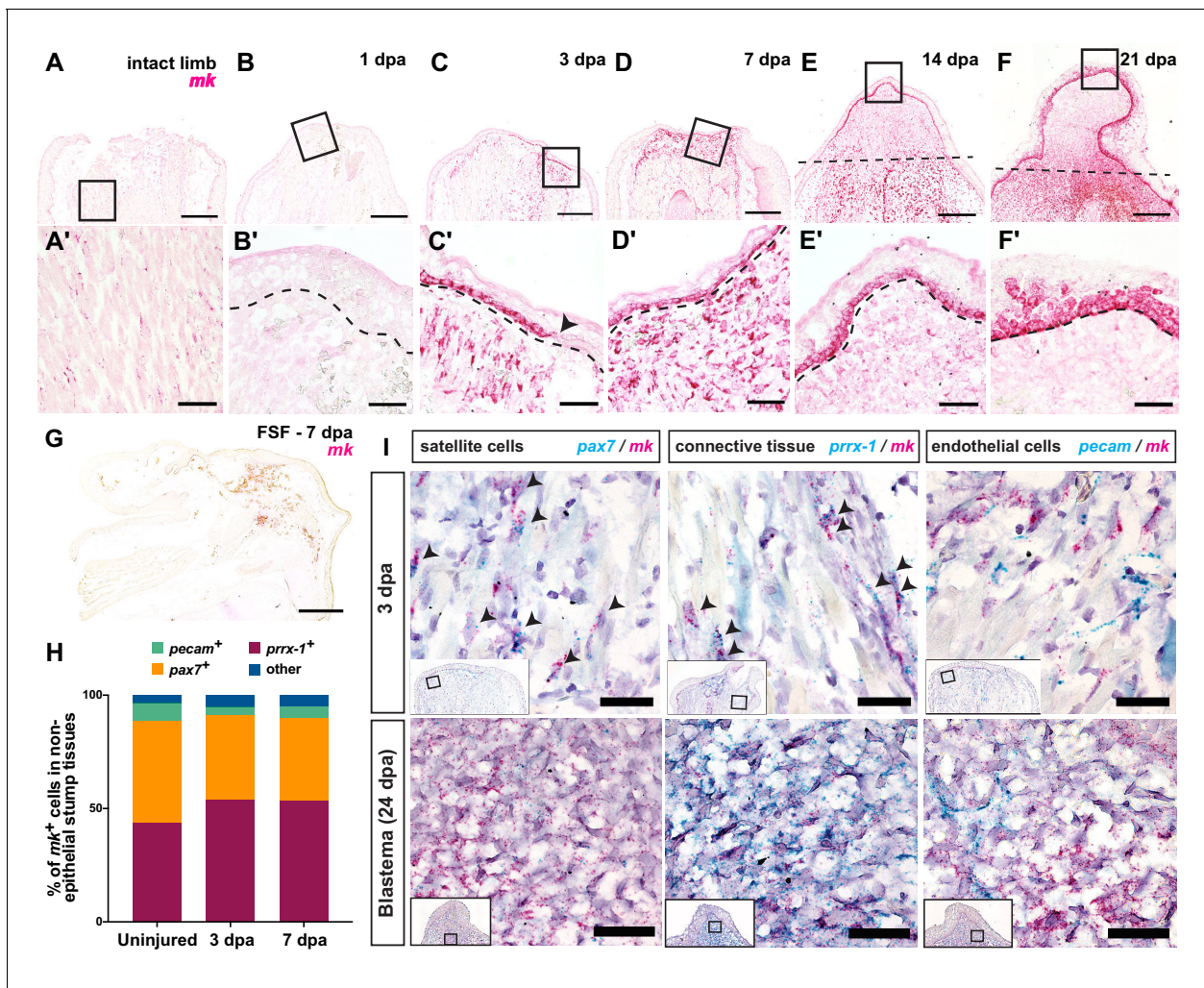


Figure 2. *Midkine* (*mk*) is highly expressed in the basal layers of the wound epidermis/AEC and blastemal progenitors. (A–F′) Timecourse RNAscope in situ hybridization of *midkine* at 0 (intact), 1, 3, 7, 14, and 21 dpa. Insets in A–F are shown in A′–F′ at higher magnification. Arrowhead in C′ denotes the beginning of the wound epidermis. Dotted line marks amputation plane in E and F or wound epidermis/AEC boundary in B′–F′. (G) In situ hybridization of *mk* in full skin flap sutured limbs at 7 dpa. Axolotl MK protein expression can be found in **Figure 2—figure supplement 1**. (H) Breakdown of the percentages of *mk*⁺ cells that are *pax7*⁺, *prrx-1*⁺, and *pecam*⁺ in regenerating stump tissues during early stages of regeneration. At 3 dpa, a total N of 1579, 444, and 1180 cells were counted for *pax7*, *prrx-1*, and *pecam* double in situs, respectively. At 7 dpa, a total N of 456, 1043, and 274 cells were counted for *pax7*, *prrx-1*, and *pecam* double in situs, respectively (**Figure 2—source data 1**). (I) Representative images of RNAscope double in situ hybridization of *mk* with *pax7* (left), *prrx-1* (middle), or *pecam* (right) at early (3 dpa) and later blastema (24 dpa) stages. Insets depict where higher magnification images were taken. Black arrowheads mark double positive cells. More detailed analysis of the onset of *mk* expression in early stages of regeneration, representative images of double in situ hybridization of *mk* with cell type-specific markers in uninjured tissue, as well as the analysis of *mk* co-expression with the monocyte marker *csf1r* can be found in **Figure 2—figure supplement 2**. Scale bars, A–G: 500 μ m, A′–F′: 100 μ m, I: 50 μ m. dpa, days post-amputation, FSF, full skin flap.

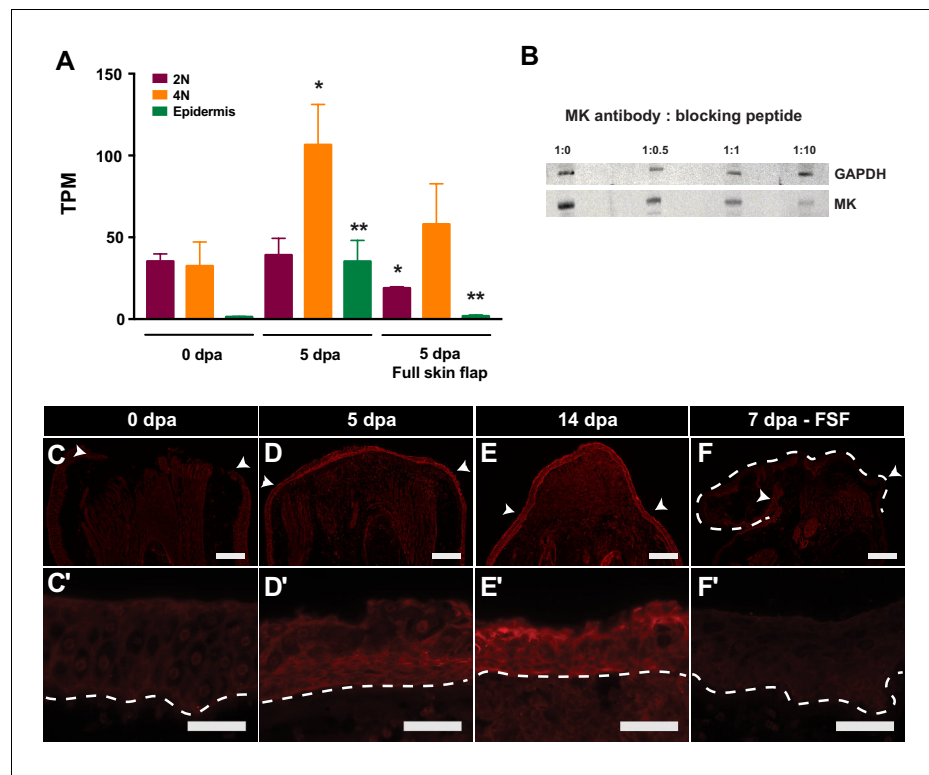


Figure 2—figure supplement 1. MK protein is found throughout the wound epidermis/AEC. **(A)** Normalized TPM levels of *midkine* (*mk*) in regenerating and full skin flap conditions. **(B)** Validation of custom polyclonal rabbit anti-MK antibody. Western blotting was performed with increasing volumetric ratios of MK antibody: blocking peptide ratios on 10 dpa protein extracts and revealed lower levels of staining with increased levels of peptide. **(C–F)** Immunostaining of axolotl MK protein at 0 (C–C'), 5 (D–D') and 14 dpa (E–E'). White arrowheads denote the amputation plane. Higher 20x magnification images of the wound epidermis or AEC (14 dpa) are shown in C'–F'. **(F–F')** Immunostaining of axolotl MK protein in full skin flap sutured limbs at 7 dpa reveals lower levels of expression. Dotted lines demarcate full skin flap in F and the wound epidermis/stump boundary in C'–F'. Graphs are mean \pm SD. ** $p < 0.005$, * $p < 0.05$. Scale bars, B, E–H: 500 μ m, E'–H': 100 μ m. FSF, full skin flap; dpa, days post-amputation.

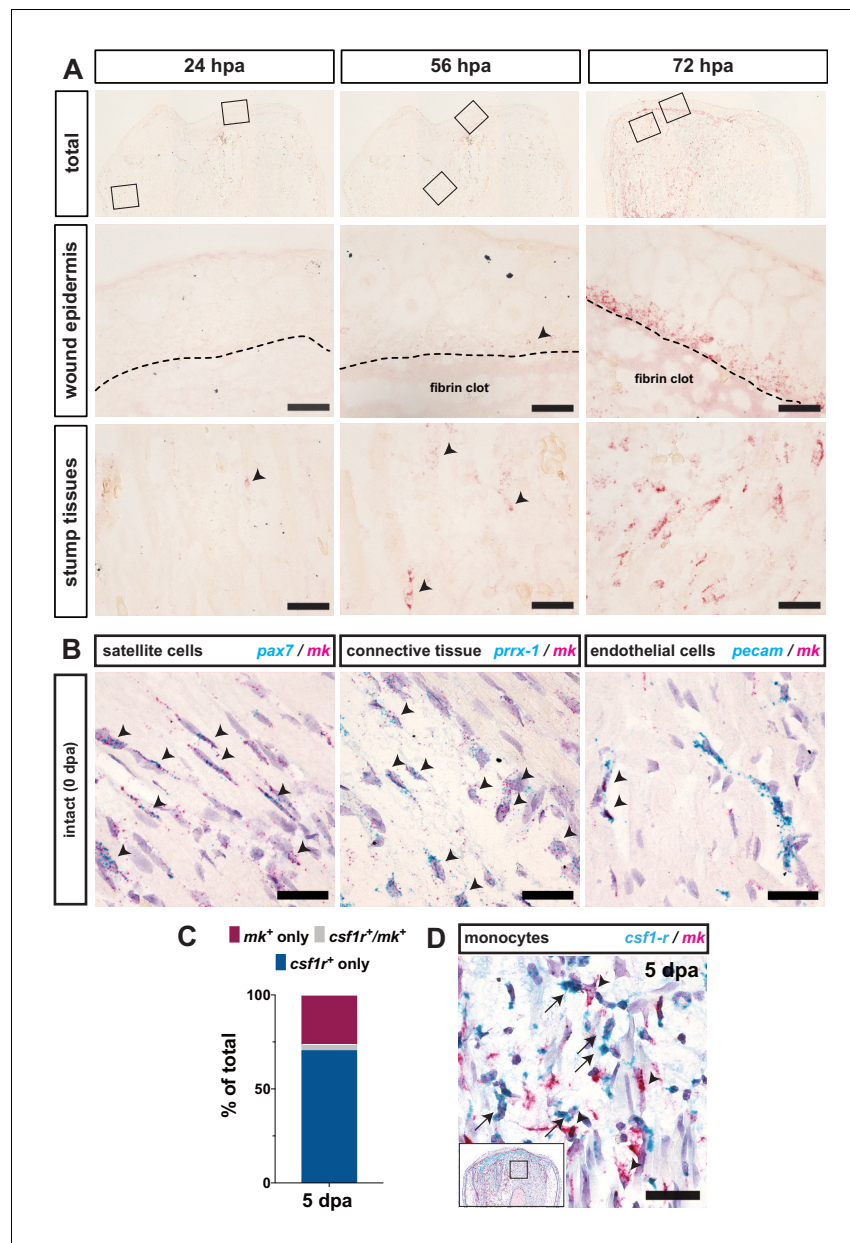


Figure 2—figure supplement 2. *Mk* is expressed in satellite cells, connective tissue, and endothelial cells in intact tissues. (A) RNAscope in situ hybridization of *mk* at 24, 56, and 72 hpa. Dotted line denotes wound epidermis boundary. Black arrowheads point to examples of *mk*⁺ cells. (B) Double RNAscope in situ hybridization of *mk* in red and *pax7* (left) (N = 1073 cells counted), *prrx-1* (middle) (N = 1723 cells counted), and *pecam* (right) (N = 1693 cells counted) in blue in non-regenerating intact limbs. Black arrowheads mark double positive cells. (C) Quantification of *mk*⁺ only, *csf1r*⁺ only, and co-positive cells. (D) Double RNAscope in situ hybridization of *mk* and *csf1r* at 5 dpa reveals discrete expression patterns (N = 582 cells counted). Black arrowheads denote *mk*⁺ only cells and black arrows denote *csf1r*⁺ only cells. Scale bars are 50 μ m. hpa, hours post-amputation, dpa, days post-amputation.

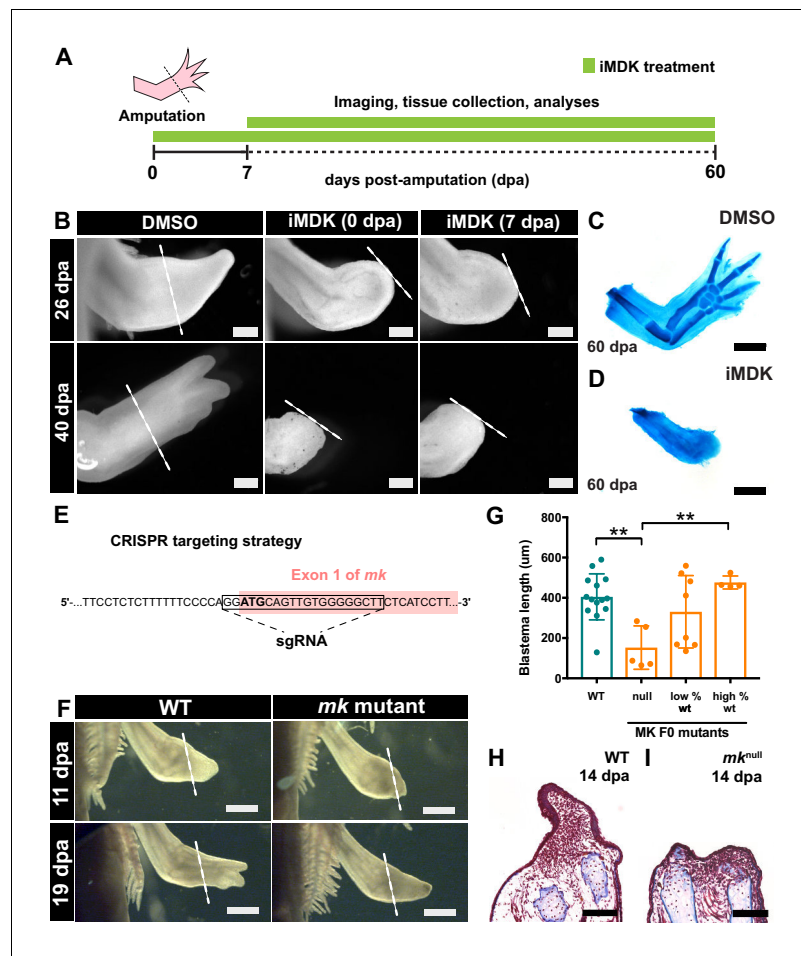


Figure 3. Chemical and genetic perturbations of *mk* impair limb regeneration. (A) Experimental design. (B) Brightfield images of DMSO- or iMDK-treated limbs (N = 4/4 iMDK-treated in each condition did not regenerate). (C–D) Alcian blue staining of DMSO- or iMDK-treated limbs at 60 dpa. (E) CRISPR strategy to target the start codon of *mk* to generate mutants. Control animals were generated using a non-targeted tracrRNA/cas9 complex and were unmodified at the *mk* locus. (F) Brightfield images of regenerating limbs from control animals or *mk* F0 mutants. (G) Quantification of blastema length at 14 dpa in control or *mk* mutant limbs. The severity of the delay in regeneration segregated based on genotype of the animal as either control (*mk*^{WT}), mosaic null (*mk*^{null}), or partially modified (low or high % WT alleles) (N = 14 control *mk*^{WT}, 5 *mk*^{null}, 8 low % WT, 4 high % WT). Graph is mean ± SD. (H–I) Representative images of picro-mallory stained sections of regenerating limbs in control animals or *mk* null mutants. Example genotyping analyses and *mk* null mutant immunofluorescence validation can be found in **Figure 3—figure supplement 1**. **p<0.005, two-tailed unpaired Student's t-test was employed. Each N represents one limb from a different animal. White dotted lines mark amputation plane. Scale bars, B–D, H–I: 500 μm, F: 1 mm. WT, wildtype, dpa, days post-amputation.

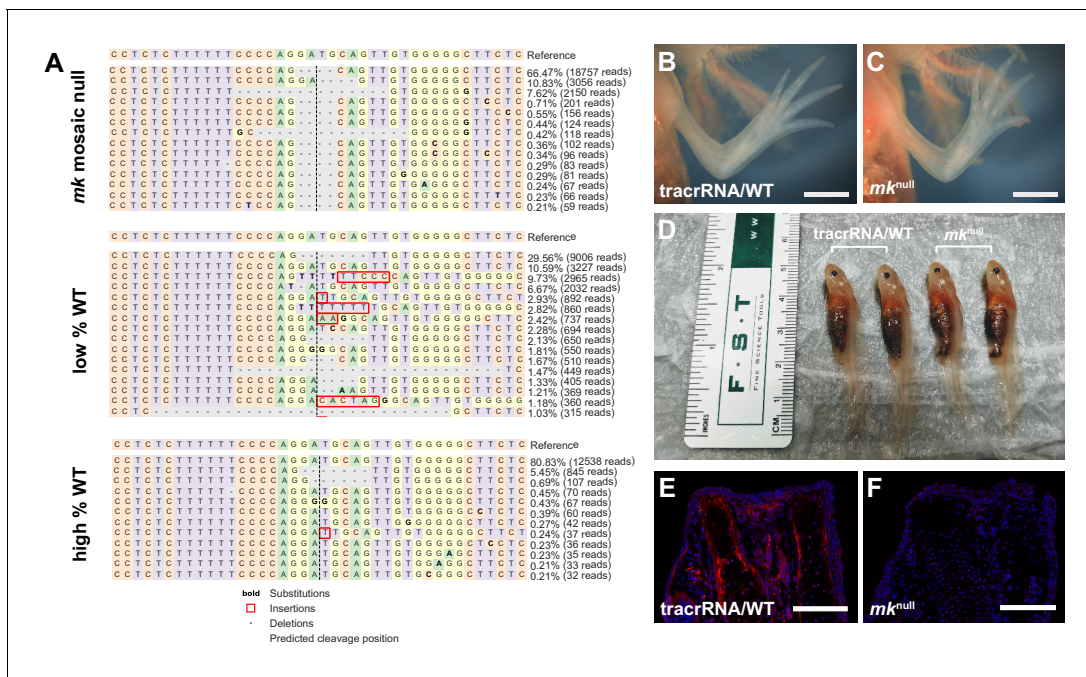


Figure 3—figure supplement 1. CRISPR generation of *mk* mosaic null mutants. (A) Example genotyping results of fully modified (mosaic null, abbreviated *mk*^{null}) or partially modified (low % or high % WT) animals. (B–C) Representative brightfield images of tracrRNA control and *mk*^{null} forelimb of four-month old sibling axolotls. (D) Side-by-side brightfield image of tracrRNA control and *mk*^{null} axolotls demonstrating no gross observational difference in body size. (E–F) Representative MK immunostaining of a tracrRNA control or *mk* mosaic null mutant at 7 dpa reveals a loss of staining. Scale bars, B–C: 2 mm, E–F: 500 μ m. dpa, days post-amputation.

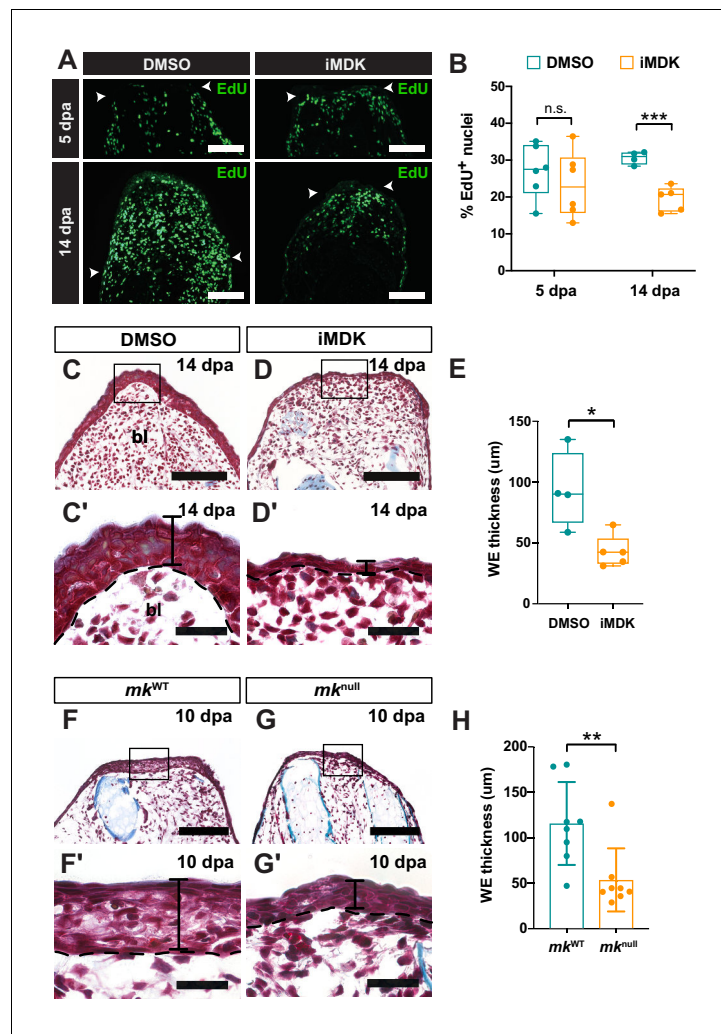


Figure 4. *Mk* perturbations result in defective AEC development. (A–B) EdU staining (A) and quantification (B) of the total percentage of EdU⁺ nuclei of DMSO/iMDK-treated limbs at 5 dpa (N = 6 DMSO, 6 iMDK) and 14 dpa (N = 4 DMSO, 5 iMDK). White arrowheads denote the amputation plane in A. (C–D') Picro-mallory stained sections from regenerating limbs from DMSO/iMDK-treated animals. Higher magnification images of the AEC are shown in C'–D'. (E) Quantification of wound epidermis (WE) thickness in DMSO/iMDK-treated regenerating limbs at 14 dpa (N = 4 DMSO, 5 iMDK). (F–G') Picro-mallory stained sections from regenerating limbs from regenerating limbs of control WT (*mk*^{WT}) or *mk*^{null} animals. Higher magnification images of the developing AEC at 10 dpa are shown in F'–G'. (H) Quantification of WE thickness in regenerating limbs of *mk*^{WT} or *mk*^{null} animals at 14 dpa (N = 8 *mk*^{WT}, 8 *mk*^{null}). Picro-mallory staining of a 40 dpa iMDK-treated limb is shown in **Figure 4—figure supplement 1**. Each N represents a limb from a different animal. Two-tailed unpaired student's t-test was used for statistical analysis. Graphs are mean ± SD. *p<0.05, **p<0.005, ***p<0.001. Scale bars, A, C–D, F–G: 200 μm, C'–D', F'–G': 100 μm. bl, blastema, dpa, days post-amputation.

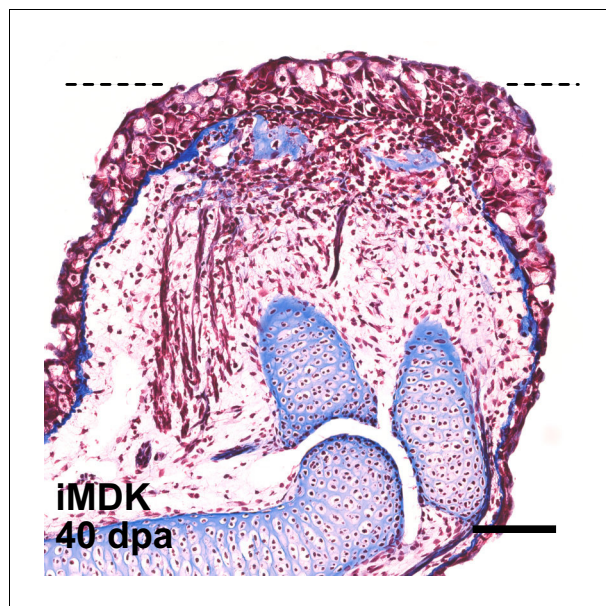


Figure 4—figure supplement 1. iMDK-treated limbs do not regenerate. Representative picro-mallory staining of a section from an iMDK-treated limb at 40 dpa. Re-formation of the blue collagen-thick dermal layer is commencing at the amputation plane (denoted with the black dotted line). Accumulation of fibroblastic blastemal cells can be seen at the amputation plane, although a blastema never forms. Scale bar, 200 μ m.

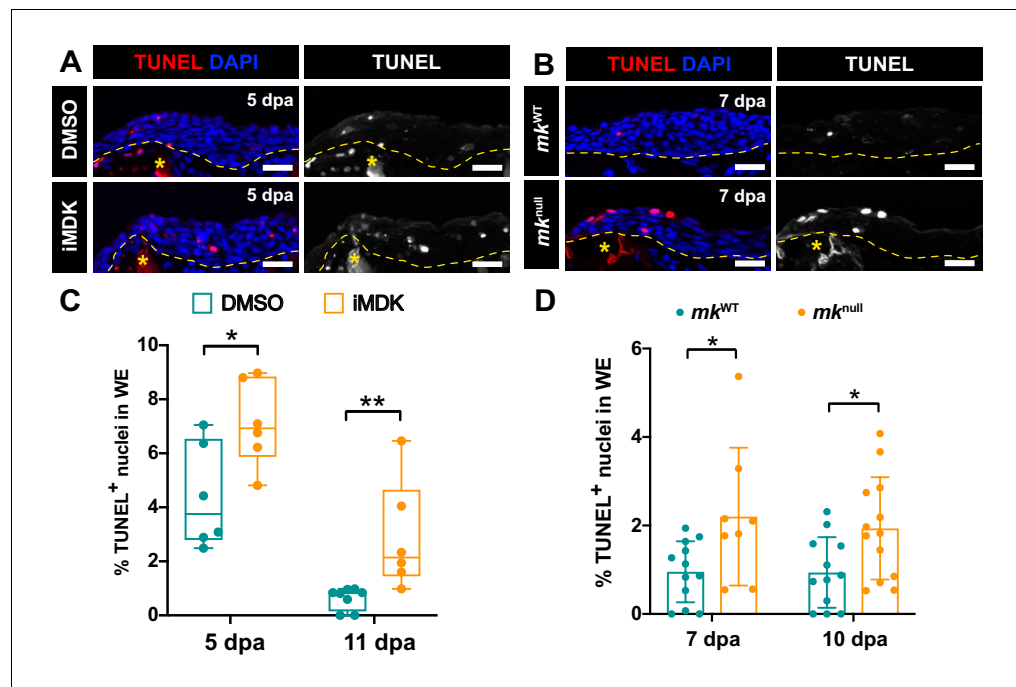


Figure 5. *Mk* acts as a critical survival factor during AEC development. (A) Representative TUNEL-stained sections from limbs of DMSO and iMDK-treated limbs. (B) Representative TUNEL-stained sections from limbs of regenerating *mk*^{WT} control or *mk*^{null} mutants. (C) Quantification of the % TUNEL⁺ nuclei in the wound epidermis of DMSO or iMDK-treated limbs at 5 dpa (N = 6 DMSO, 6 iMDK) or 11 dpa (N = 8 DMSO, 6 iMDK). (D) Quantification of the percentage of TUNEL⁺ nuclei in *mk*^{WT} control and *mk*^{null} mutants at 7 dpa (N = 12 *mk*^{WT}, 8 *mk*^{null}) and 10 dpa (N = 12 *mk*^{WT}, 13 *mk*^{null}). Asterisks mark auto-fluorescent bone. Each N represents a limb from a different animal. Quantification of levels of blastemal cell death in DMSO/iMDK-treated and *mk*^{WT}/*mk*^{null} regenerating limbs can be found in **Figure 5—figure supplement 1**. Two-tailed unpaired student's t-tests were used for statistical analysis. Graphs are mean \pm SD. *p<0.05, **p<0.005. Scale bars: 100 μ m. dpa, days post-amputation.

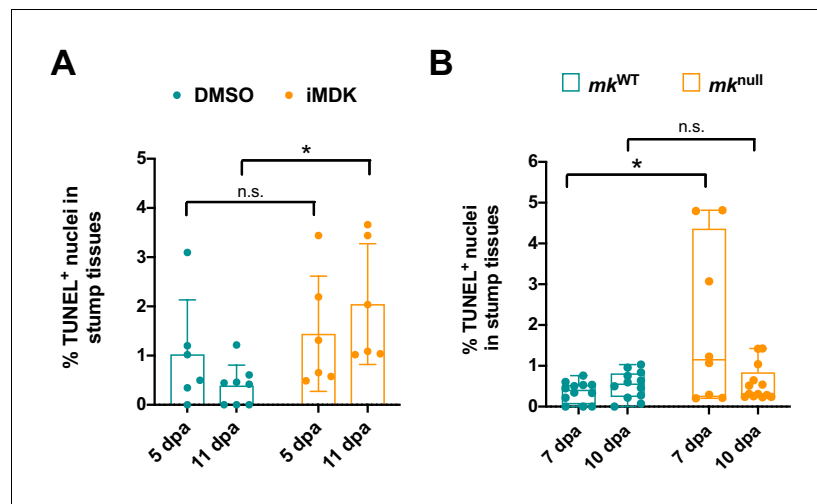


Figure 5—figure supplement 1. *Mk* is not required for blastemal cell survival. (A–B) Quantification of the percentage of TUNEL⁺ nuclei in blastemal cells of regenerating stump tissues in DMSO/iMDK-treated (5 dpa: N = 6 DMSO, 6 iMDK; 11 dpa: 8 DMSO, 6 iMDK) (A) or wildtype/*mk*^{null} mutant (7 dpa: N = 12 *mk*^{WT}, 8 *mk*^{null}; 10 dpa: N = 12 *mk*^{WT}, 13 *mk*^{null}) (B) regenerating limbs reveals iMDK-treated limbs exhibit higher consistent levels of cell death, whereas *mk* mutant limbs are able to resolve cell death. Two-tailed unpaired t-tests were performed at each time point between the two conditions for statistical analysis. Graphs are mean ± SD. *p<0.05. n.s., not significant; dpa, days post-amputation.

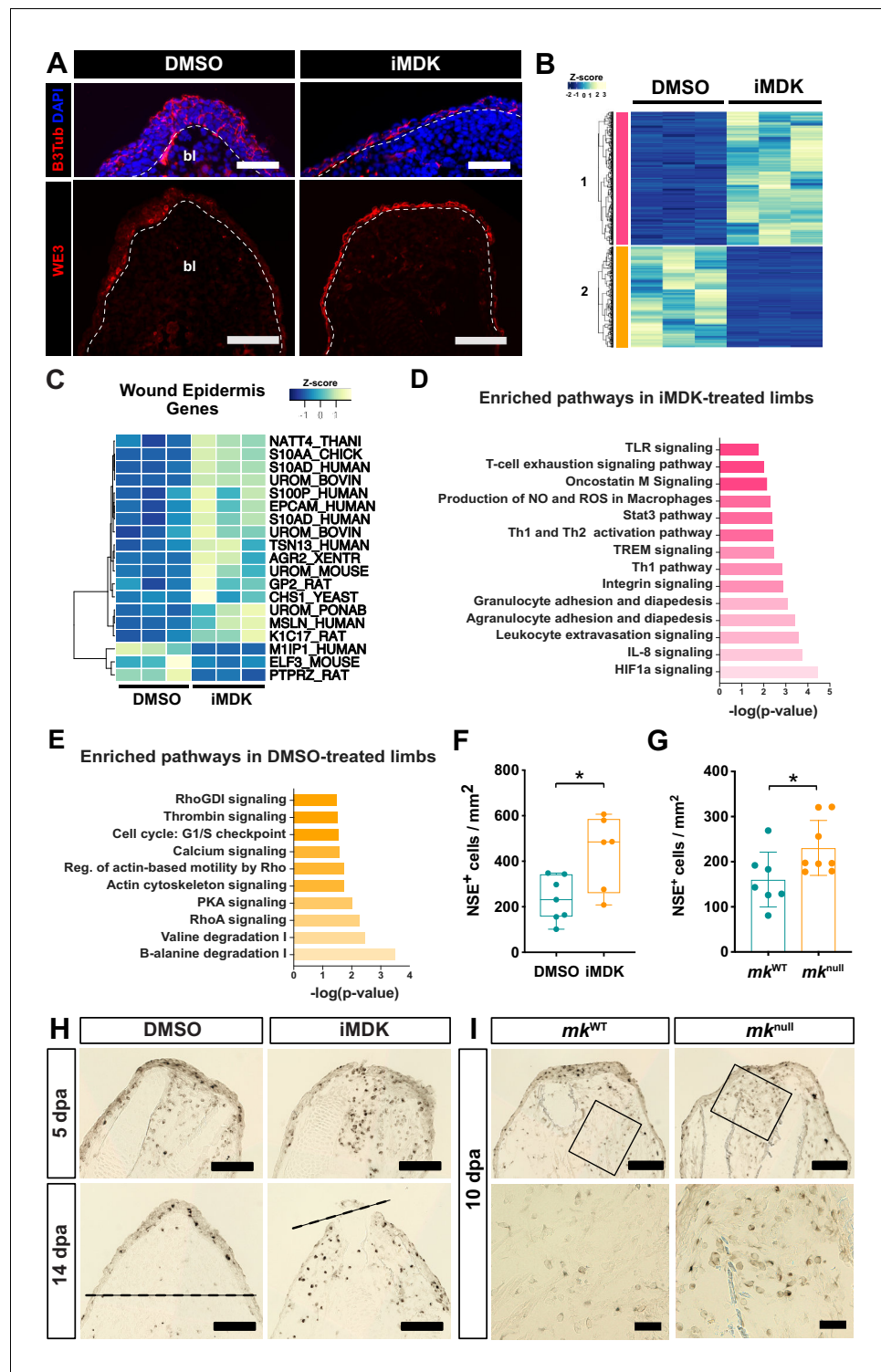


Figure 6. iMDK-treated and *mk* mutant regenerating limbs display dysregulated wound epidermis gene expression and persistent inflammation. (A) Beta-III tubulin staining or WE3 staining of DMSO- or iMDK-treated limbs. White dotted line marks boundary of wound epidermis/AEC-blastema. (B) Heatmap of annotated differentially expressed transcripts in DMSO- and iMDK-treated limbs ($N = 3$ each) reveals two main clusters (colored pink and orange) of transcripts either enriched in DMSO or iMDK treatments. Transcript expression was normalized per row and plotted as a Z-score. Differentially expressed transcripts can be found in **Supplementary file 4**. (C) Heatmap of normalized TPM expression levels of wound epidermis genes in DMSO- or iMDK-treated limbs. (D) Bar graph of enriched pathways in iMDK-treated limbs. (E) Bar graph of enriched pathways in DMSO-treated limbs. (F) Dot plot of NSE⁺ cells/mm² in DMSO- and iMDK-treated limbs. (G) Dot plot of NSE⁺ cells/mm² in *mk*^{WT} and *mk*^{null} limbs. (H) Histology of DMSO- and iMDK-treated limbs at 5 and 14 dpa. (I) Histology of *mk*^{WT} and *mk*^{null} limbs at 5 and 10 dpa. Figure 6 continued on next page

Figure 6 continued

iMDK-treated regenerating limbs at 11 dpa. (D) Plot of enriched pathways in iMDK-treated limbs. (E) Plot of enriched pathways in DMSO-treated limbs. (F) Quantification of NSE⁺ monocytes at 5 dpa in DMSO/iMDK-treated limbs at 5 dpa (N = 7 DMSO, 6 iMDK). (G) Quantification of the density of NSE⁺ monocytes in *mk*^{WT} control and *mk*^{null} regenerating limbs at 10 dpa (N = 7 *mk*^{WT}, 8 *mk*^{null}). (H) NSE staining of DMSO- and iMDK-treated limbs at 5 dpa and 14 dpa. Dotted lines demarcate the amputation plane. (I) Representative NSE stained sections from regenerating limbs of *mk*^{WT} control and *mk*^{null} mutants at 10 dpa. Higher magnification insets are shown in bottom two panels. Each N represents a limb from a different animal. Data demonstrating rescue of *mk*^{null} phenotypes via overexpression of *mk* during regeneration in mutant limbs as well as electroporation efficiency metrics can be found in **Figure 6—figure supplements 1, 2 and 3**. A two-tailed unpaired student's t-test was used for statistical analysis. Graphs are mean ± SD. *p<0.05. Scale bars, A (top): 100 μm, A (bottom), H-I (top): 200 μm, I (bottom): 50 μm. bl, blastema, dpa, days post-amputation.

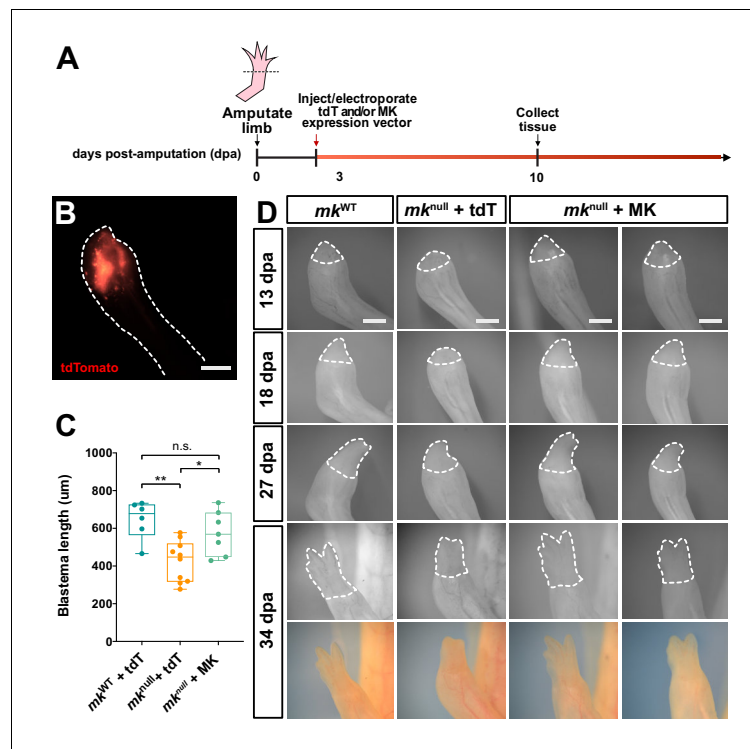


Figure 6—figure supplement 1. *Mk* overexpression in mk^{null} regenerating limbs rescues delayed regeneration. (A) Experimental schematic of rescue experiment. Either a pCAG-MK and/or pCAG-tdTomato control overexpression construct was injected and electroporated into the regenerating limbs of wildtype or mk^{null} animals at 3 dpa. (B) Representative image of tdTomato fluorescence in a pCAG-MK/pCAG-tdTomato co-electroporated regenerating limb at 14 dpa (outlined in white dotted line). (C) Quantification of blastema length at 13 dpa. One-way ANOVA analyses were employed on each set of data for statistical analysis (N = 6 mk^{WT} + tdT, 10 mk^{null} + tdT, 7 mk^{null} + MK). (D) Representative time course images of regenerating mk^{WT} and mk^{null} limbs electroporated with pCAG-tdTomato and/or pCAG-MK constructs. Two different rescue animals are shown here. Graphs are mean \pm SD. **p<0.005, *p<0.05. Scale bars, B, D: 1 mm. n.s., not significant; dpa, days post-amputation.

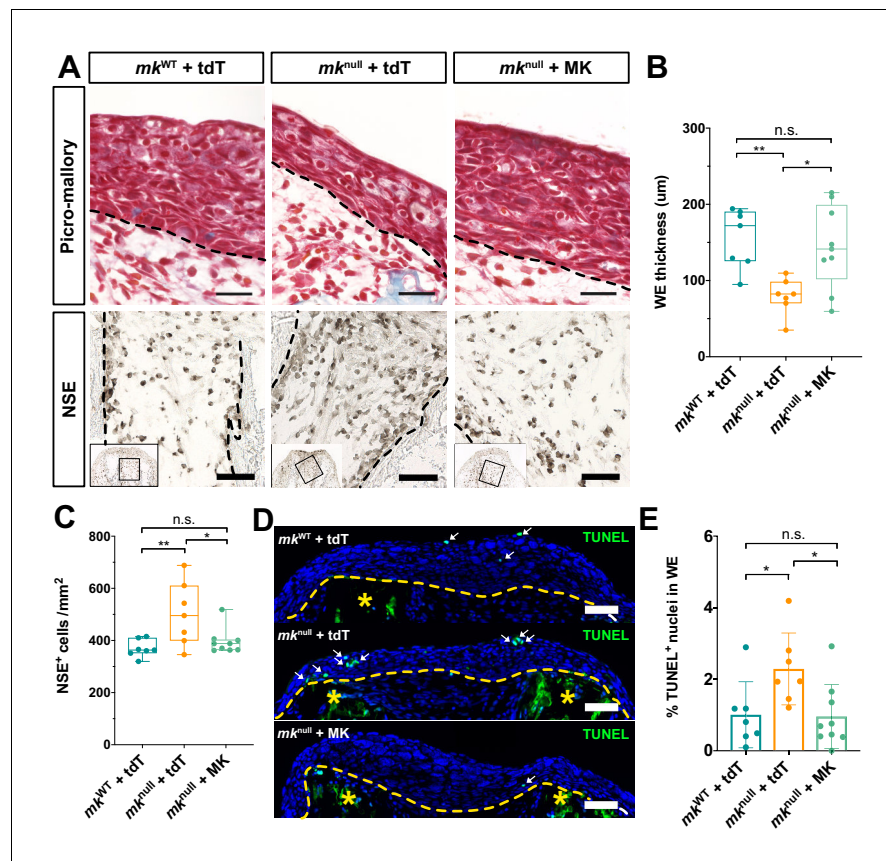


Figure 6—figure supplement 2. *Mk* overexpression in *mk*^{null} regenerating limbs rescues mutant wound epidermis and monocyte density phenotypes. (A) Representative images of picromallory-stained (top row) and NSE-stained (bottom row) sections from tdTomato and/or *mk*-overexpressing wildtype and mutant regenerating limbs. Black dotted lines mark the wound epidermis or bone boundary in the top and bottom rows, respectively. (B) Quantification of wound epidermis thickness at 10 dpa. (C) Quantification of NSE⁺ monocyte density at 10 dpa. (D) Representative images of TUNEL-stained sections, focusing on the wound epidermis. Yellow dotted line demarcates the boundary between the wound epidermis and regenerating stump tissues. Yellow asterisk marks the auto-fluorescent bone. White arrows point to green TUNEL⁺ nuclei. (E) Quantification of TUNEL⁺ nuclei in the wound epidermis at 10 dpa. One-way ANOVA analyses were employed on each set of data for statistical analysis (N = 7 *mk*^{WT} + tdT, 7 *mk*^{null} + tdT, 9 *mk*^{null} + MK). Graphs are mean ± SD. **p<0.005, *p<0.05. Scale bars, B (top row), 50 μm, B (bottom row) and D, 100 μm. n.s., not significant; dpa, days post-amputation.

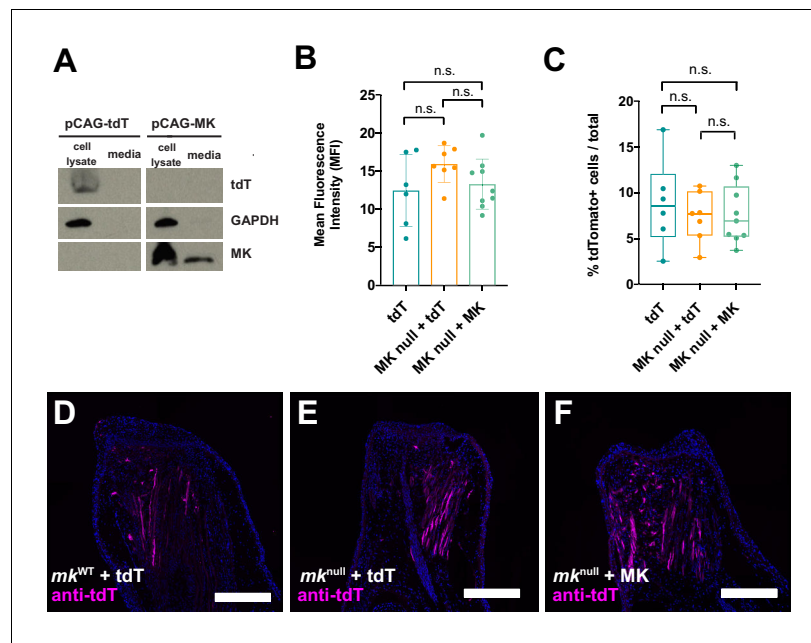


Figure 6—figure supplement 3. Electroporation efficiencies are similar between pCAG-tdTomato and pCAG-MK injected *mk^{null}* mutant and *mk^{WT}* regenerating limbs. (A) Validation of pCAG-MK overexpression construct with MK antibody. Western blots of either pCAG-tdTomato or pCAG-MK transfected 293 T cells with the custom axolotl-MK antibody reveals the overexpression and secretion of axolotl MK in pCAG-MK, but not pCAG-tdTomato (tdT), transfected cell lysates and media. (B–C) Quantification of mean fluorescence intensity and the percentage of tdTomato⁺ expressing cells out of total DAPI⁺ cells in the distal-most 500 μ m of regenerating tissue at 10 dpa. (D–F) Representative images of anti-tdTomato-stained sections from each condition. One-way ANOVA analyses were employed on each set of data for statistical analysis (N = 7 *mk^{WT}* + tdT, 7 *mk^{null}* +tdT, 9 *mk^{null}* + MK). Scale bars, 500 μ m. dpa, days post-amputation, n.s. not significant.

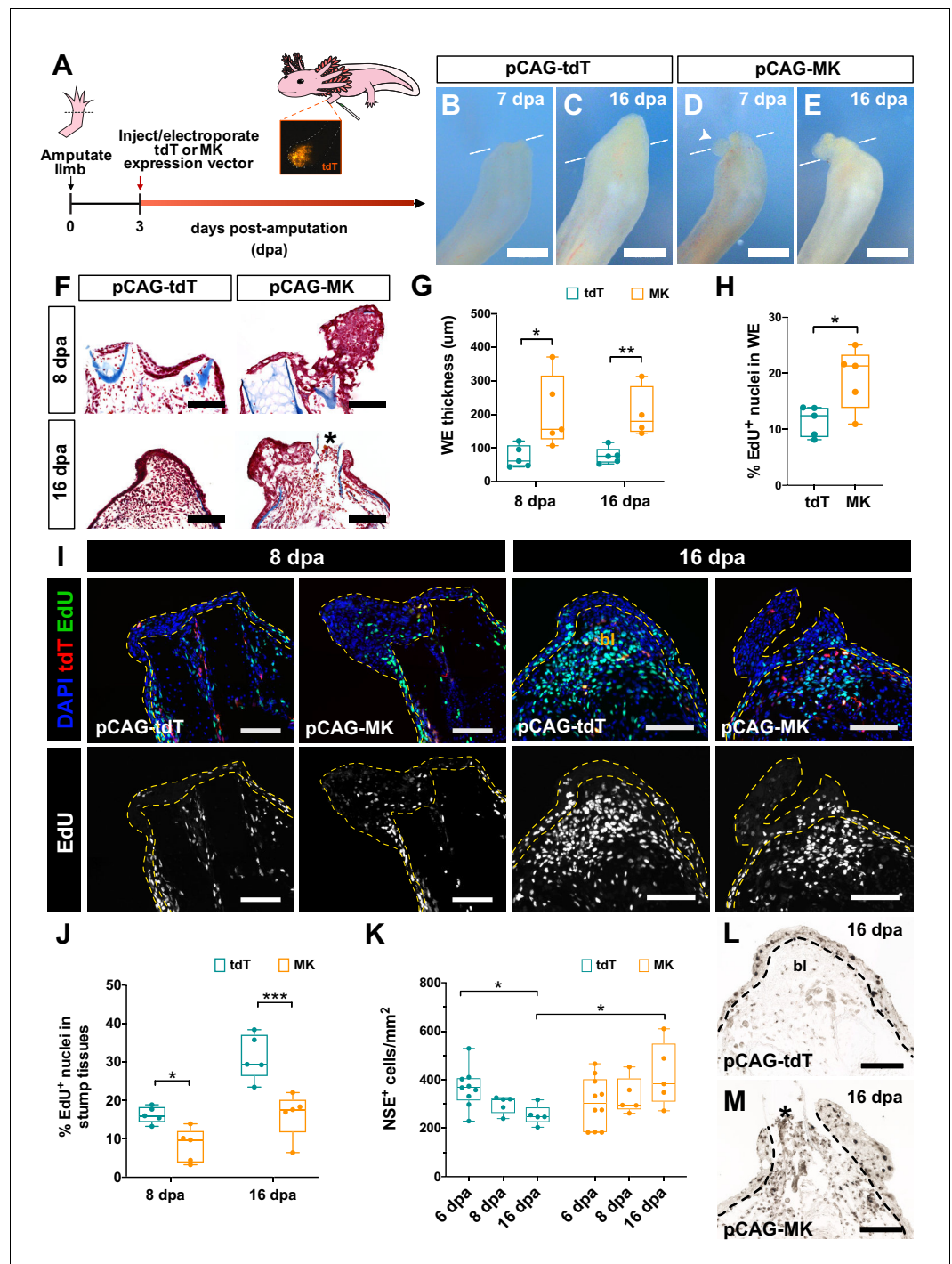


Figure 7. Overexpression of *mk* in regenerating limbs leads to wound epidermis expansion, decreased blastemal cell proliferation, and improper resolution of inflammation. (A) Schematic of *mk* overexpression experiment. (B–E) Representative brightfield images of tdTomato (tdT)- (B–C) or *mk*-overexpressing (D–E) regenerating limbs at 7 and 16 dpa. White dotted line denotes amputation planes and white arrowhead in D denotes small aberrant skin growth. (F) Representative picromallory stained sections of tdT- or *mk*-overexpressing regenerating limbs. Asterisk marks protruding bone. (G) Quantification of wound epidermis thickness in tdTomato- or *mk*-overexpressing limbs at 8 dpa (N = 5 each) and 16 dpa (N = 5 tdT, N = 4 MK). (H) Quantification of the percentage of EdU⁺ nuclei in the wound epidermis of tdTomato- or *mk*-overexpressing limbs at 8 dpa (N = 5 each). (I) Representative images of EdU-stained sections of tdTomato- or *mk*-overexpressing limbs. Wound epidermis/AEC are outlined with yellow dotted lines. (J) Quantification of the percentage of EdU⁺ nuclei in

Figure 7 continued on next page

Figure 7 continued

regenerating stump tissues of tdT- or *mk*-overexpressing limbs. (K) Quantification of the density of NSE⁺ monocytes in tdT- or *mk*-overexpressing limbs. (L–M) Representative images of NSE-stained sections in tdT- or *mk*-overexpressing limbs. Black dotted line denotes wound epidermis boundary. Asterisk denotes protruding bone. Quantification of EdU⁺ cells in the wound epidermis and blastemal cells of DMSO/iMDK-treated and WT/*mk*^{null} regenerating limbs is shown in **Figure 7—figure supplement 1**. Electroporation efficiency data can be found in **Figure 7—figure supplement 2**. Data showing that *mk*-overexpressing regenerating limbs display delayed regeneration is shown in **Figure 7—figure supplement 3**. Data demonstrating that overexpression of *mk* in non-regenerating intact limbs does not affect cellular proliferation or monocyte density can be found in **Figure 7—figure supplement 4**. Graphs are mean ± SD. Two-tailed unpaired student's t-tests were used for statistical analysis. *p<0.05, **p<0.01, ***p<0.005. Scale bars, B-E: 500 μm, F, I, L-M: 200 μm. bl, blastema, dpa, days post-amputation.

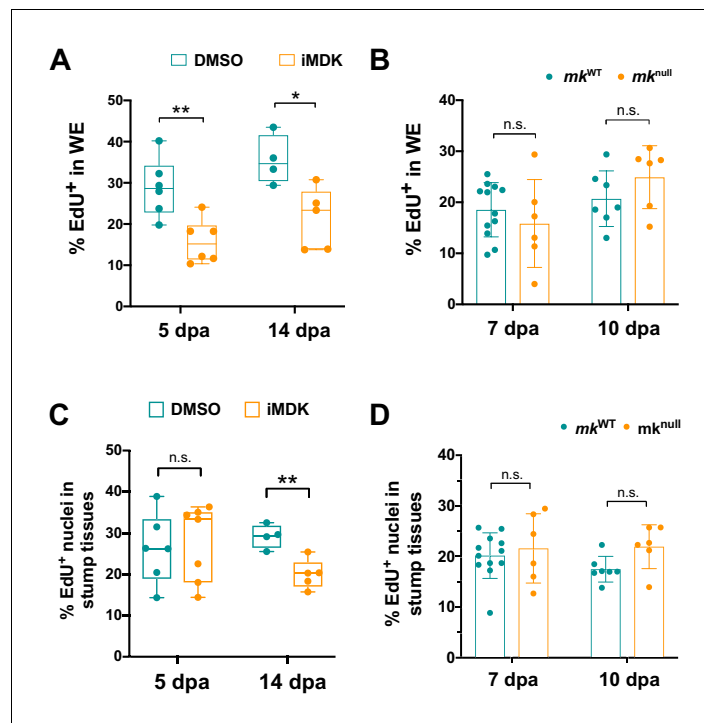


Figure 7—figure supplement 1. *Mk* is not required for proliferation in the wound epidermis or blastemal cells. (A–B) Quantification of the percentage of EdU⁺ cells in the wound epidermis (WE) of DMSO/iMDK-treated limbs (5dpa: N = 6 DMSO, 6 iMDK; 14 dpa: N = 4 DMSO, 5 iMDK) (A) or *mk*^{WT}/*mk*^{null} limbs (7 dpa: N = 12 *mk*^{WT}, 8 *mk*^{null}; 10 dpa: N = 12 *mk*^{WT}, 13 *mk*^{null}) (B). (C–D) Quantification of the percentage of EdU⁺ blastemal cells in DMSO/iMDK-treated limbs (C) or *mk*^{WT}/*mk*^{null} limbs (D). Two-tailed unpaired t-tests were performed at each time point between the two conditions for statistical analysis. Graphs are mean ± SD. **p < 0.005, *p < 0.05. n.s., not significant; dpa, days post-amputation.

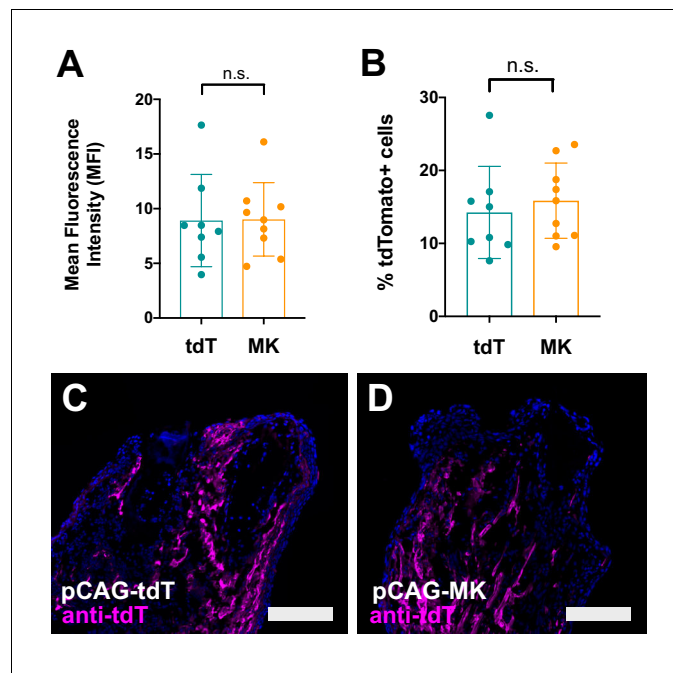


Figure 7—figure supplement 2. Electroporation efficiencies of pCAG-tdT and pCAG-MK injected regenerating limbs are similar. (A–B) Quantification of mean fluorescence intensity (MFI) (A) and the percentage of tdTomato⁺ cells out of the total DAPI⁺ cells (B) in the distal most 500 μ m of regenerating pCAG-tdT (N = 8) and/or pCAG-MK (N = 9) electroporated limbs at 6 dpa. (C–D) Representative immunostaining against tdTomato of tdTomato⁺ or MK-electroporated limbs. Two-tailed unpaired t-tests were performed for statistical analysis. Scale bar, 250 μ m. dpa, days post-amputation, n.s., not significant.

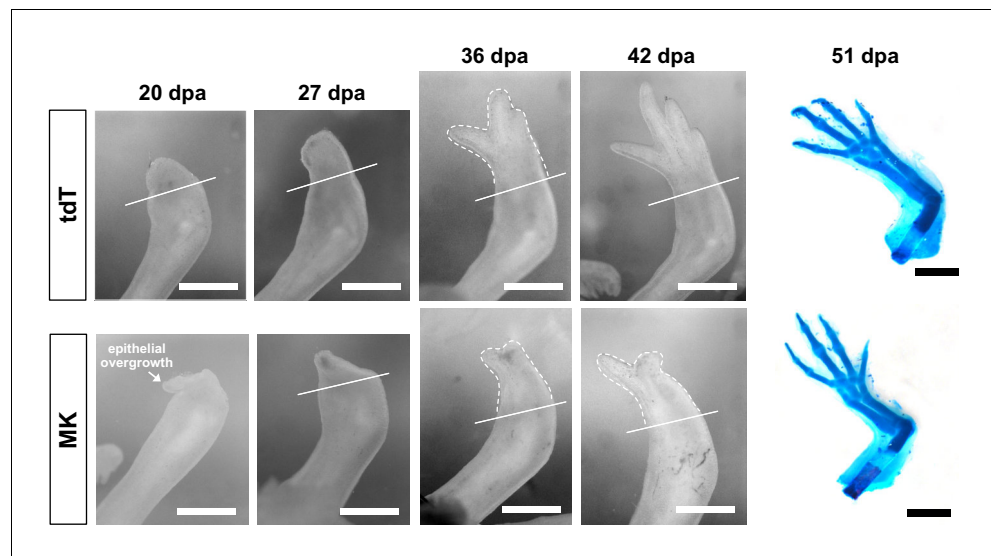


Figure 7—figure supplement 3. *Mk*-overexpressing limbs resolve epithelial overgrowth and undergo delayed regeneration. Representative time course images of control tdTomato (top) or *mk*-overexpressing (bottom) regenerating limbs at 20, 27, 36, and 42 dpa (N = 9/12 animals exhibited a substantial delay in regeneration). Alcian-stained regenerated limbs at 51 dpa are shown on the far right. Scale bars, 1 mm. dpa, days post-amputation.

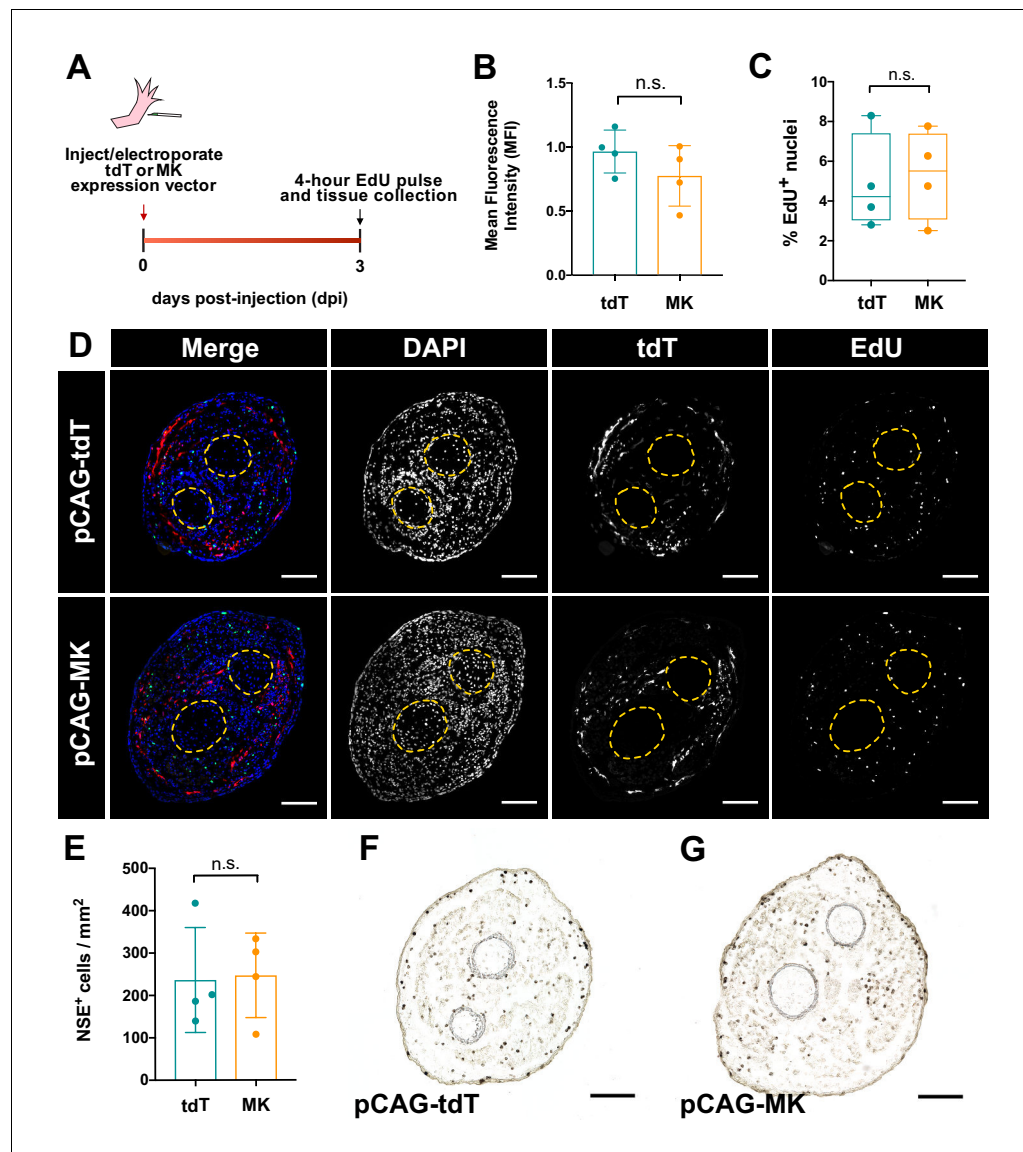


Figure 7—figure supplement 4. Overexpression of *mk* in non-regenerating intact limbs does not affect cellular proliferation or monocyte density. (A) Experimental schematic of overexpression experiment in non-regenerating limbs. (B) Mean fluorescence intensity (MFI) quantification of electroporated limbs. (C) Quantification of the percentage of EdU⁺ cells in tdT- or *mk*-overexpressing intact limbs. (D) Representative images of tdT and EdU-stained cross-sections from electroporated limbs. (E) Quantification of monocyte density in overexpression limbs. (F–G) Representative images from NSE⁺ stained sections from non-regenerating overexpression limbs. Two-tailed unpaired t-tests were performed for statistical analysis. Graphs are mean ± SD. Scale bars, D, F–G: 200 μm. n.s., not significant.

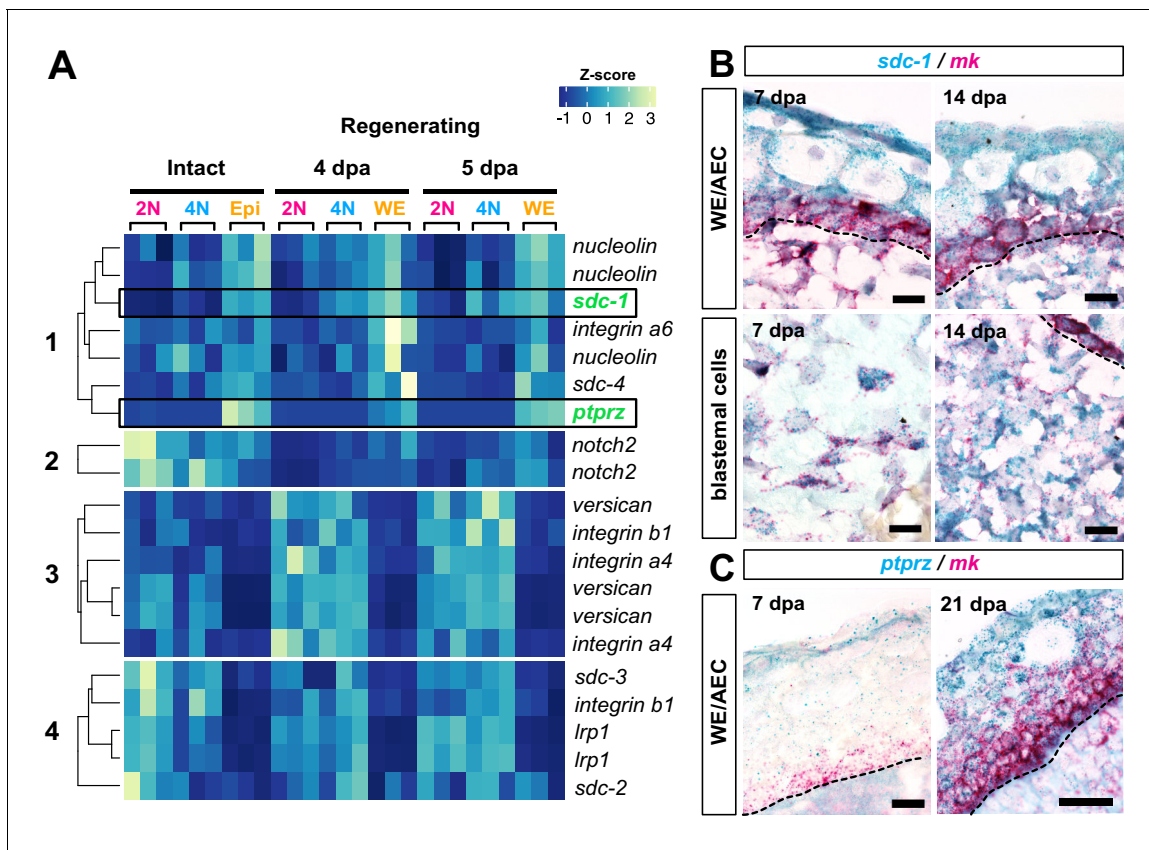


Figure 8. *Mk* receptors are expressed throughout regenerating tissues. (A) Heatmap of normalized transcript levels for expressed *mk* receptors in intact and regenerating subpopulations from our RNA-seq dataset revealed four general patterns of expression (**Figure 8—source data 1**). (B–C) Double RNAscope in situ hybridization of *mk* (bright red puncta) with its cognate receptors *sdca-1* (B) or *ptprz* (C) (dark blue puncta). Dotted black line denotes wound epidermis/AEC boundary. Since *ptprz* expression was low during early stages of regeneration, *ptprz/mk* in situ were performed without a hematoxylin counterstain to ease visualization of dark blue puncta in the wound epidermis at 7 dpa. Scale bars, B and C (left panel): 25 μ m for 63x magnification, C (right panel): 50 μ m for 40x magnification. WE, wound epidermis, AEC, apical epithelial cap, bl, blastema, dpa, days post-amputation.

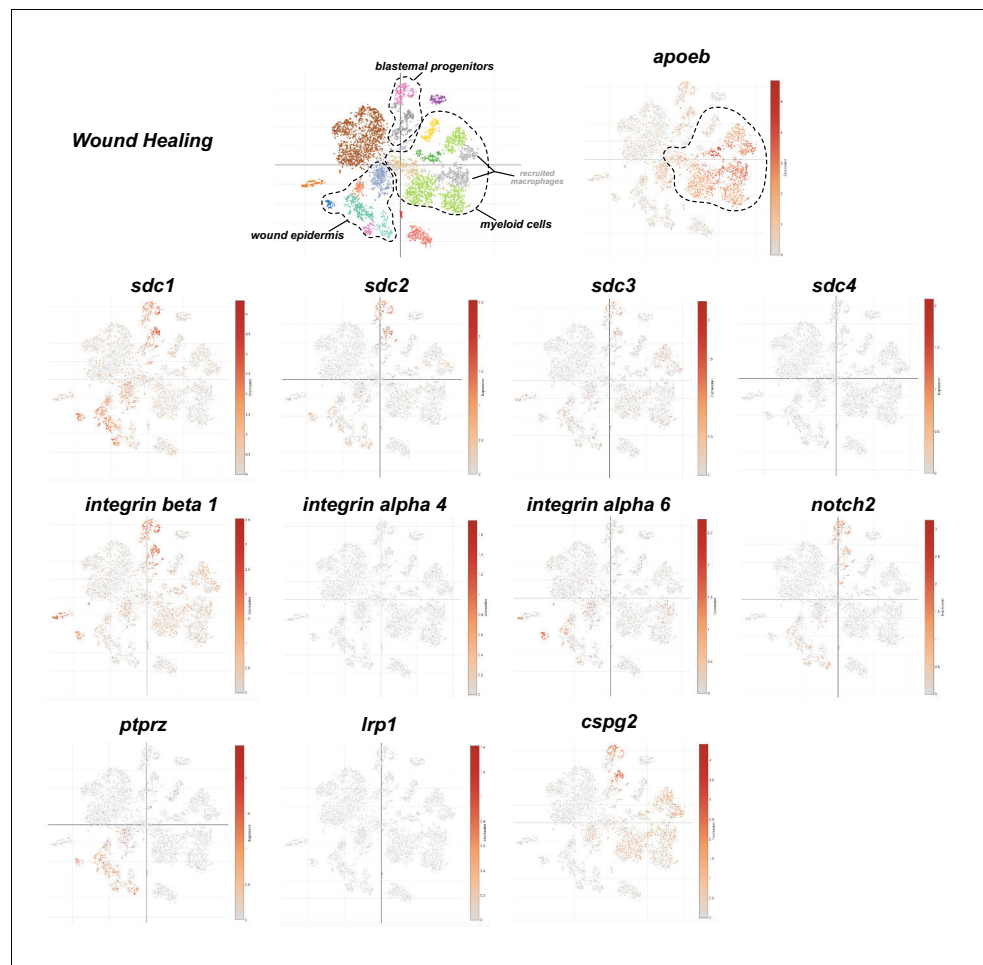


Figure 8—figure supplement 1. *Mk* receptors are not highly expressed in myeloid cells during wound healing. Publicly available single cell expression data of *mk* receptors from [Leigh et al. \(2018\)](#). Top left panel shows original clustering of single cell expression profiles at the wound healing stage of blastemal progenitors, wound epidermis, and myeloid cell populations circled. Top right panel shows t-SNE plot of *apoeb* expression, which was identified as highly enriched in myeloid cells, to give an example of a highly expressed gene in the myeloid cell populations. All panels below are t-SNE plots showing expression of *mk* receptors.